THE JOURNAL OF PHYSICAL CHEMISTRY B

Article

Ultrafast Energy Transfer Dynamics of a Bioinspired Dyad Molecule

Janne Savolainen, Niels Dijkhuizen, Riccardo Fanciulli, Paul A. Liddell, Devens Gust, Thomas A. Moore, Ana L. Moore, Jrgen Hauer, Tiago Buckup, Marcus Motzkus, and Jennifer L. Herek

J. Phys. Chem. B, **2008**, 112 (9), 2678-2685 • DOI: 10.1021/jp0757199

Ultrafast Energy Transfer Dynamics of a Bioinspired Dyad Molecule

Janne Savolainen,*,† Niels Dijkhuizen,† Riccardo Fanciulli,† Paul A. Liddell,‡ Devens Gust,‡ Thomas A. Moore,‡ Ana L. Moore,‡ Jürgen Hauer,§ Tiago Buckup,§ Marcus Motzkus,§ and Jennifer L. Herek†,||

FOM Institute for Atomic and Molecular Physics (AMOLF), Kruislaan 407, 1098 SJ Amsterdam, The Netherlands, Department of Chemistry and Biochemistry, Arizona State University, Tempe, Arizona 85287, Physichalische Chemie, Fachbereich Chemie, Philipps-Universität, 35032 Marburg, Germany, and Optical Sciences Group, Department of Science and Technology, MESA+ Institute for Nanotechnology, University of Twente, Enschede 7500 AE, The Netherlands

Received: July 20, 2007; In Final Form: November 14, 2007

A caroteno−purpurin dyad molecule was studied by steady-state and pump−probe spectroscopies to resolve the excited-state deactivation dynamics of the different energy levels as well as the connecting energy flow pathways and corresponding rate constants. The data were analyzed with a two-step multi-parameter global fitting procedure that makes use of an evolutionary algorithm. We found that following ultrafast excitation of the donor (carotenoid) chromophore to its S_2 state, the energy flows via two channels: energy transfer (70%) and internal conversion (30%) with time constants of 54 and 110 fs, respectively. Additionally, some of the initial excitation is found to populate the hot ground state, revealing another limitation to the functional efficiency. At later times, a back transfer occurs from the purpurin to the carotenoid triplet state in nanosecond timescales. Details of the energy flow within the dyad as well as species associated spectra are disentangled for all excited-state and ground-state species for the first time. We also observe oscillations with the most pronounced peak on the Fourier transform spectrum having a frequency of 530 cm^{-1}. The dyad mimics the dynamics of the natural light-harvesting complex LH2 from *Rhodopseudomonas acidophila* and is hence a good model system to be used in studies aimed to further explain previous work in which the branching ratio between the competing pathways of energy loss and energy transfer could be manipulated by adaptive femtosecond pulse shaping.

Introduction

In photosynthetic plants and algae, the early time energy transfer (ET) between two chromophores (from carotenoid molecules to porphyrin molecules) is the key step in making use of the energy of the blue−green photons of sunlight in photosynthesis.[1] In a photosynthetic light-harvesting complex of *Rhodopseudomonas acidophila*, a photosynthetic purple bacteria (Figure 1a), energy is transferred from rhodopin glucoside carotenoids to bacteriochlorophyll *a* molecules. In this particular system, the efficiency of ET from the donor (carotenoid) to the acceptor (bacteriochlorophyll) is about 56%, while the rest of the harvested energy is dissipated via the intramolecular process of internal conversion (IC).[2−4] Previously, Herek and co-workers demonstrated that, by using adaptive femtosecond pulse shaping, it is possible to attain coherent control over the branching ratio between the two competing pathways.[5] The relative efficiencies of the two processes, the functional pathway (ET) and the loss channel (IC), could be manipulated by 30%. The features of the potential energy surfaces, and the detailed pathways of the energy flow in the natural light-harvesting complex LH2, are critical factors in understanding the mechanisms leading to this control. However, this system is comprised of several chromophores of both types, embedded in a large protein, and the size becomes a problem in describing the system by means of molecular modeling.

In this work, to better understand the mechanism of coherent control, we proposed an experimental method to investigate the mechanisms behind the LH2 control study by controlling a simpler model system, comprised of only an acceptor and a donor molecule.[6] As a preparatory step to the coherent-control experiments, we performed a detailed ultrafast transient-absorption study of a caroteno−purpurin dyad model system (Figure 1c) and compared the structure, spectra, and dynamics to that of LH2.

We begin with a structural description of LH2 and the dyad. The crystal structure of LH2 has already been determined to atomic resolution.[7] LH2 consists of nine subunits, arranged in a ring structure, each including three bacteriochlorophyll (Bchl) molecules and one rhodopin glucoside carotenoid (Car) molecule, all embedded and noncovalently bound to the surrounding protein. The Bchl molecules are arranged in two rings that are physically and spectrally different. According to the maxima of their Q_y absorption peak, they are called the B800 and B850 BChls. Each carotenoid has an S-like conformation and interacts with the neighboring Bchls in two protomers. The distance from the carotenoid π-conjugated stem to the Bchl-B800 macrocycle is ∼3.4 Å and ∼3.6 Å to the Bchl-B850. In comparison, the dyad has only a single carotenoid and a single purpurin, covalently linked together by an amide group (Figure 1c). The

* Corresponding author. Tel.: +31 20 608 1234; fax: +31 20 668 4106; e-mail: savolainen@amolf.nl.
† AMOLF.
‡ Arizona State University.
§ Philipps-Universität.
|| University of Twente.

10.1021/jp0757199 CCC: $40.75
Published on Web 02/09/2008

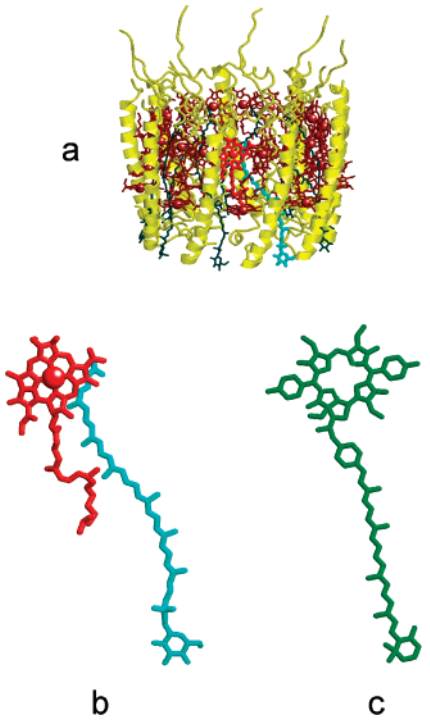

Figure 1. Structure of LH2 pigments as compared to the dyad. (a) LH2, (b) expansion of two highlighted pigments in panel a (the carotenoid donor in blue and the porphyrin acceptor in red), and (c) schematic structure of the carotenopurpurin dyad; the donor and acceptor are chemically bridged by an amide link.

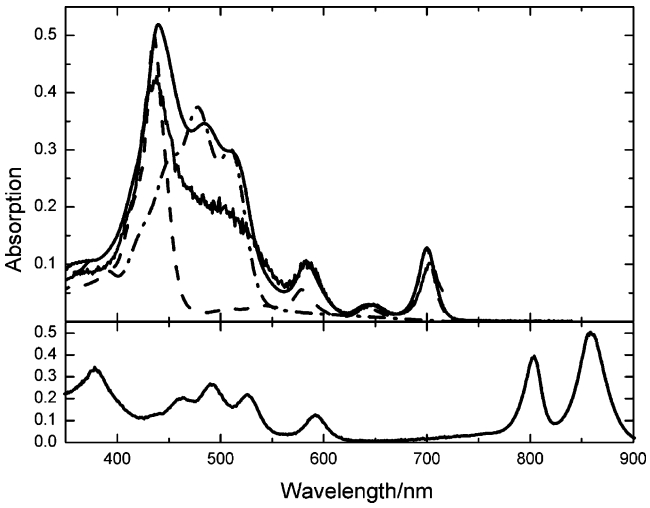

Figure 2. Upper panel: absorption spectra of the dyad (solid line), carotenoid (dashed−dotted line), purpurin (dashed line), and excitation spectrum of the dyad (gray line). Lower panel: absorption spectrum of the LH2 complex from *R. acidophila*.

distance from the edge of the π-conjugation of the carotenoid to the edge of the π-conjugation of the purpurin ring is ∼3.7 Å.

Despite these structural dissimilarities, the dyad mimics the major spectral features of the LH2 complex well. The steady-state spectra of both systems consist of overlapping carotenoid and purpurin (Bchl in LH2) bands, depicting their well-known features (see Figure 2). Both LH2 and dyad show a characteristic three-peak structure in the region of 400−550 nm, corresponding to the carotenoid absorption. The peak of the 0−0 vibrational band of the carotenoid S_2 state in the dyad (∼520 nm) is slightly blue shifted relative to that of LH2 (∼525 nm), and the same trend is seen in the purpurin/Bchl Q_x bands (583 nm vs 590 nm). In LH2, the position of the Bchl Q_y band is strongly dependent on the embedding of the pigment in the two distinct binding sites of the protein (800 or 850 nm). Further, excitonic coupling in the B850 ring affects the line shape of the absorption band.[2] In solution, the difference is much less: Bchl absorbs at ∼770 nm, while the purpurin tetrapyrrole is at ∼700 nm. More important is that the Q_x bands, which are primarily involved in the ET process from the carotenoids, are overlapping.

To probe the degree of similarity between the LH2 and the dyad, we focused on the function of LH2 as a light-harvesting complex. Only by showing a similarity in the internal dynamics of ET in the two molecules can we really conclude that our model system is a good candidate for investigating the previous results of coherent control. Critical in this analysis are details of carotenoid photophysics that were proposed to play a crucial role in the control experiments in LH2.[8] Hence, we made it our priority to identify the spectral signatures belonging to the different species involved in the dynamics and to understand the pathways, and their efficiencies, related to ET from the carotenoid to the purpurin.

In the case of LH2, the pathways and related rate constants have been previously described in detail by many studies.[2,3,9] According to the generally accepted energy-flow model, about 51% of the absorbed energy in this particular light-harvesting complex is transferred to the accepting Bchl states (to B850 Bchls in about 190 fs and to B800 Bchls in about 280 fs). The ET process can be described to be first-order by a Förster mechanism.[2] The rest of the energy is from the carotenoid S_2 state and is dissipated via intramolecular vibrational redistribution within about 120 fs down to the so-called dark S_1 excited electronic state of the carotenoid. This process is enhanced by a conical intersection between the S_2 and the S_1 states of the carotenoid.[10] In the LH2 complex, about 20% of the energy is transferred from the carotenoid S_2 state to the B800 Bchls and about 31% to the B850 Bchls. The energy transferred to B800 will subsequently arrive to the B850 ring Bchls. In addition, a small amount of the energy (about 5%) is transferred from the S_1 state of the carotenoids to the B800 Bchls, giving a total efficiency of about 56% for ET from the carotenoid to the Bhcls.[3]

The biomimetic dyad molecule has been characterized previously by Macpherson et al., by using pump−probe, fluorescence up-conversion, and time correlated single photon counting techniques.[11] Results show that in the dyad, approximately 70% of the energy is transferred to the purpurin moiety after excitation of the carotenoid portion of the molecule with a 488 nm laser pulse. According to their analysis, all of the energy is transferred from the S_2 state of the carotenoid. Unfortunately, the time resolution in these experiments was about 3 times longer than the fastest resolved rate constant. In similar systems, it was shown that some of the energy is also transferred from the S_1 state of the carotenoid, depending on the conjugation length of the carotenoid.[12] Since the publication of ref 11 in 2002, considerable interest in carotenoid reaction dynamics has shifted to the presence and role of additional (dark) states (i.e., the hot ground state or fleeting intermediate states).[13−15] To date, no discussion on the involvement of the hot ground state or additional carotenoid excited states and their role in the photophysics of the dyad has been presented, nor has any previous study extracted the spectra belonging to the different spectral species involved in the dyad photophysics.

In the LH2 coherent-control experiments, a possible mechanism is the activation of a backbone vibrational mode of the carotenoid favoring the loss channel by directing the wave

packet on the excited state toward the conical intersection between S_2 and S_1 states.[8] Carotenoid molecules in LH2 are embedded in the protein by noncovalent interactions, which may lead to augmentation of the importance of such skeletal modes on the branching of the energy flow. This raises the question as to whether the dyad exhibits similar low-frequency modes, and if so, what role might they play in the early time photophysics? Further, is the efficiency of ET from the carotenoid to the purpurin in the dyad in solution dependent on these modes? Is it possible to activate such modes of the dyad by impulsive Raman scattering (IRS) as is the case in the LH2 complex?

In the coherent-control experiments, the feedback signal from the molecule will be resolved by means of pump−probe spectroscopy. The resulting transient-absorption spectra are a sum of many overlapping signals, originating from excited-state absorption, stimulated emission, and bleach signals of different spectral species, each depicting unique spectral and temporal characteristics. Previously, the data analysis of the pump−probe data was based on so-called single trace fitting,[11] and no global analysis of transient-absorption data has been reported on this system. A thorough understanding of the interplay of different signals contributing to the transient absorption is essential for any future studies that utilize these signals. For example, for the purposes of the coherent-control experiments, it is important to extract a reliable feedback signal that correlates with the process(es) one aims to control. In this study, we used a global fitting procedure to unravel the complex data by using a spectro-temporal model.[16]

The caroteno−purpurin dyad (Figure 1) is a model system that mimics the salient features of the natural photosynthetic complex well, while preserving structural simplicity. A complete/global characterization of the photophysics of this system is described in this article; it will be advantageous in the interpretation of coherent-control experiments.

Experimental Procedures

The caroteno−purpurin dyad was prepared according to published procedures.[11]

Steady-state absorption spectra were measured with a Jasco V-530 spectrophotometer, with the sample in a 0.5 mm rotating cuvette (built in-house) used in the pump−probe experiments. Corrected fluorescence excitation and emission spectra were obtained using a SPEX Fluorolog 112 and optically dilute samples ($A < 0.07$ in toluene). The excitation spectrum was corrected using a correction file obtained with the parent purpurin methyl ester by assuming that the absorption and fluorescence excitation spectra were identical.[7]

The pump−probe setup was as follows: Part of the output of an amplified Ti:sapphire (Clark CPA-2001) laser was coupled into a noncollinear optical parametric amplifier (NOPA), which produced ~10 μJ near-transform-limited pulses at 510 nm with ~28 nm fwhm and 18 fs pulse duration; these pulses were used as the pump pulses. A small fraction of the residual fundamental light was focused to a 2 mm sapphire window to create a white light continuum (WLC) that provided spectrally broad probe pulses ranging from 450 to 710 nm. To avoid any anisotropy effects, the polarization angle between the pump and the probe pulses was set to the magic angle (54.7°). The two beams were focused and overlapped at the sample position, where the fwhm of the Gaussian intensity profile of the pump beam was 250 μm. The pulse energy was set to 100 nJ with an adjustable filter, giving $\sim 5 \times 10^{14}$ photons cm^{-2}. The sample cuvette was rotated sufficiently quickly to provide a fresh sample for every pulse to avoid sample degradation or the accumulation of long-living states. The probe pulses were coupled into a spectrograph (Acton), and individual spectral components were focused onto a 256 pixel diode array. Diode signals were read out and AD converted at a rate of 1 kHz, thus obtaining shot-to-shot statistics for each measured spectra. Spectral resolution of the detection system was approximately 1 nm/pixel.

The time resolution of the pump−probe experiments as well as the amount of spectral dispersion in the WLC was determined by measuring the sum-frequency-mixing signal of the pump and probe pulses at the sample position in a 25 μm thick BBO crystal. The wavelength to be mixed from WLC was selected by tuning the phase matching angle of the crystal; in this way, the mixing of different wavelengths of the WLC could be measured. The time resolution was ~70 fs across the spectrum, and the overall time delay between the blue and the red parts of the WLC spectrum (chirp) was approximately ~300 fs. The measured chirp curve was used to remove the WLC dispersion from the data prior to analysis.

Spectroscopy-grade toluene was purchased from Riedel-DeHaën and used without further purification. The optical density used in the pump−probe experiments was 0.3 OD at 510 nm in the 0.5 mm path-length rotating cuvette. To check for any sample degradation, the steady-state absorption spectrum was measured before and after the measurements. No changes in the OD or spectral shapes were observed, indicating sample stability. All measurements were performed at room temperature.

Data Analysis. Temporally and spectrally resolved data were analyzed globally using analysis software developed in-house. The principles of the method were first described by Holzwarth[16] and further refined and used by van Grondelle's group.[17] Recently, a development adding the use of evolutionary algorithms to unravel the deactivation pathways in LH2 of *Rhodopseudomonas acidophila* was reported by Wohlleben et al.[18] Here, we further extend this approach by introducing a powerful covariance-matrix adaptation of an evolutionary algorithm allowing a large number of parameters.[19,20]

In the first step, the data are fitted using a so-called sequential model where the 2-D surface is described by a number of evolution associated difference spectra (EADS) that evolve sequentially and irreversibly from one to another. The free parameters in this step are the rate constants (i.e., the lifetimes) of each EADS and their spectral shapes. This provides us with preliminary information on the timescales that are involved in the kinetics as well as where they are represented spectrally.

In the second step, various more elaborate models are tested (target analysis). The goal of the target analysis is to resolve the SAS that belong to each excited state that depicts a transient spectrum and the rate constants and the deactivation pathways connecting these states. These models are comprised of parameters for the initial distribution of population (states (de)populated by the excitation pulse), rate constants connecting the states and SAS. Ground-state bleach signals are described by inverted absorption spectra, having only their amplitude as a free parameter. The spectral profiles of the rest of the SAS were each described by 50 parameters, using a small weighting factor, based on the second derivative of the spectra, to favor smooth spectral shapes.

The fitting proceeds within a learning loop, where the target objective is to find the spectro-temporal model that, together with corresponding rate constants, best fits the data. The quality of the fit is evaluated by its χ^2 value. The program employs an algorithm based on evolutionary principles. We start with a generation of 20 random sets of parameters, corresponding to

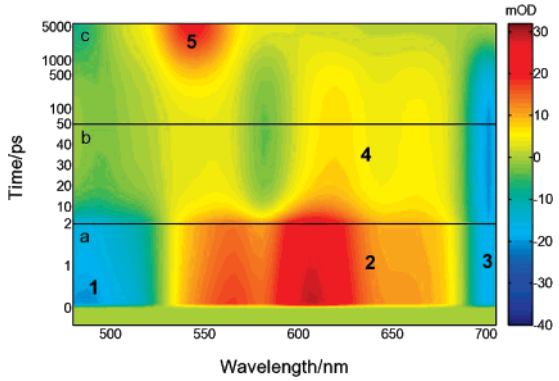

Figure 3. Pump−probe data as a function of time (*y*) and wavelength (*x*). The characteristic features of Car bleach (1), Car S1 ESA (2), Pur Bleach (3), Pur ESA (4), and Car triplet ESA (5) are indicated. Note the three different time axes. a: 0−2 ps, linear; b: 2−50 ps, linear; and c: 50 ps −to 6.2 ns (logarithmic).

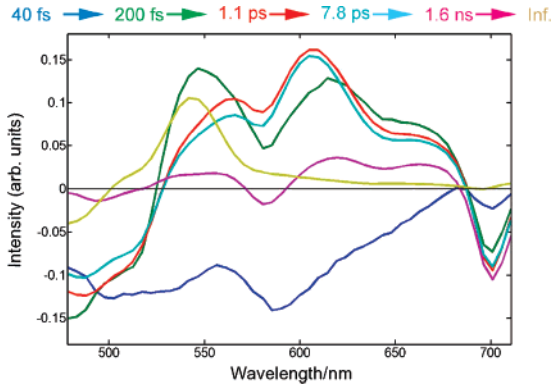

Figure 4. Results of the global analysis using the sequential model. The following EADS are shown: 40 fs (dark blue), 200 fs (green), 1.1 ps (red), 7.8 ps (light blue), 1.58 ns (magenta), and infinite (beige).

20 simulated surfaces, comparing the surfaces to the measured data and evaluating their χ^2 values. On the basis of this information, a new generation of individuals is created by the algorithm. The iteration is then left to run until convergence to an acceptable χ^2 value is reached and the measured data are simulated sufficiently. Details of the fitting program and examples will be presented elsewhere.

The errors in the resolved time constants (and quantum yields) were determined using the variance in several fits resulting in comparable χ^2 values.

Results

Steady-State Measurements. Absorption spectra of the dyad, the reference carotenoid, and the reference purpurin (all dissolved in toluene) are shown in Figure 2, along with the LH2 spectrum for comparison. Essentially, the dyad spectrum is a sum of the absorption of the two contributing chromophores, showing the first optically allowed transition of the carotenoid from the ground state to the S_2 state between 350 and 550 nm with its vibrational substructure, as well as the Soret, Q_x, and Q_y absorption bands of the purpurin with maxima at 439, 583, and 699 nm, respectively. In the dyad, the amplitude of the Q_x band is slightly enhanced and shifted 5 nm to the red as compared to the isolated purpurin in solution. Also, the Soret band shows a minor red shift in the dyad. The vibrational substructure in the absorption of the carotenoid moiety is reduced as compared to the free Car in solution.

The fluorescence excitation spectrum of the dyad was measured to determine the efficiency of the singlet−singlet ET. Figure 2 shows the fluorescence excitation spectrum of the dyad, normalized with the linear absorption spectrum at the maximum of the Q_x band (583 nm), where all of the absorption is due to the purpurin. From the ratio between these normalized spectra, in the region where the carotenoid absorption dominates (460−515 nm), the yield of the ET is on average 67%.

Time-Resolved Measurements. To characterize the energy flow pathways following the excitation by the pump pulse, we performed spectrally resolved ultrafast transient-absorption measurements, where the time delay between pump and probe pulses was scanned from negative times to 6.2 ns and the broad band probe light was detected from 470 to 710 nm. The resulting 2-D pump−probe data are shown in Figure 3.

After the excitation, five major contributions are visible. At early times, the negative signal on the blue side of the measured spectral range coincides spectrally with the carotenoid steady-sate absorption (1); the strong positive signal in the central region of the measured spectral range (2) is due to an excited-state absorption; and the negative signal at ∼700 nm originates from the bleach of the Q_y transition of the purpurin moiety (3). Further, the bleach signal due to the Q_x band of the purpurin is seen as a crevice carved at 580 nm on the positive excited-state absorption extending from 520 to 690 nm.

A major part of the positive excited-state absorption (ESA) as well as the carotenoid bleach signal decays during the first 20 ps. A broad and weak positive signal in the central region remains together with the features of the purpurin bleach (4). A small rise of the negative signal at 700 nm can be seen. At the later times, as the positive signal between 600 and 690 nm and the negative signal at 700 nm both decay on nanosecond timescales, a new positive band arises, peaking at 540 nm (5). This is accompanied by a slight increase of the negative signal on the blue side of the measured spectrum (Figure 3c, top left corner).

It is evident that various signals are superimposed. This congestion and/or overlap of signals causes difficulties in the data analysis. For example, the so-called single-trace fitting results in a multi-exponential function, of which physical interpretation may become an intractable problem.[16,17] To extract quantitative and physically interpretable information out of the measured pump−probe data, we made use of a global fitting procedure described in the Experimental Procedures.

To determine the number of time constants involved in the overall spectral evolution, the data were fitted using a simple sequential model. The model consists of a number of states evolving subsequently to the next one with time. The related spectra are left to develop without any constraints as the fitting proceeds. In principle, this approach is purely mathematical and requires no physical intuition or previous knowledge of the system, both of which may well be a hindrance to an objective data analysis. Hence, this approach provides a beneficial way to begin to unravel the kinetics of any molecular system. In this first step, the pump−probe surface is expressed by so-called EADS and the corresponding lifetimes that link the spectra together (e.g., the third EADS rises with the second lifetime and decays with the third). The found EADS (Figure 4) are used in concert with the experimental data to provide the first insights into the kinetics of the dyad molecule.

To aid the description of the rich dynamics, depicting features ranging from femtosecond to nanosecond timescales, the data are presented here in three different time regimes: early (0−2 ps), medium (2−50 ps), and late time ranges (50 ps to 6.2 ns). The pump−probe surface and the temporal cuts are plotted accordingly (regions a−c in Figures 3 and 6). From the pump−probe surface (Figure 3), accompanying spectral and temporal

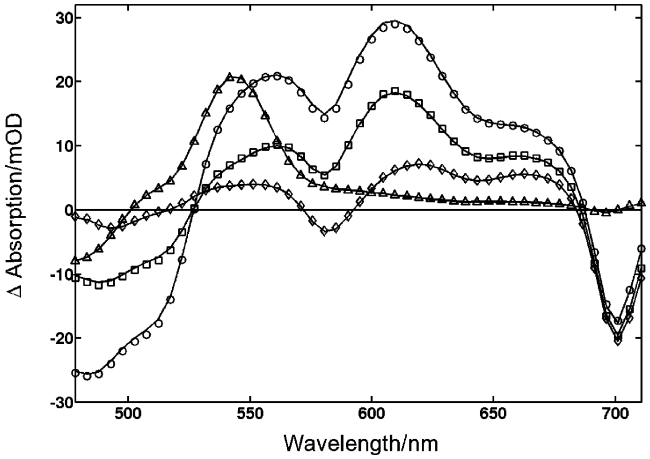

Figure 5. Spectral sections of the pump−probe data (symbols) at selected time delays together with the fit (solid line): 420 fs (circles), 7 ps (squares), 50 ps (diamonds), and 6.2 ns (triangles).

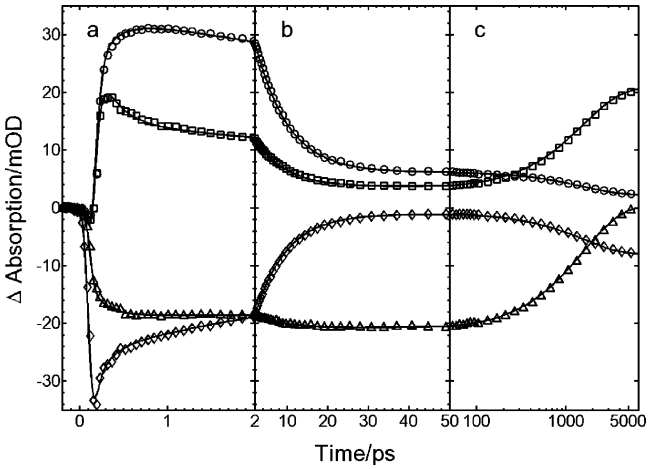

Figure 6. Time traces of the pump−probe data (symbols) at selected wavelengths, together with the fit (solid line): 478 nm (diamonds), 546 nm (squares), 610 nm (circles), and 700 nm (triangles). Note the three different time axes. a: 0−2 ps, linear; b: 2−50 ps, linear; and c: 50 ps −to 6.2 ns (logarithmic).

sections (Figures 5 and 6) as well as EADS (Figure 4), the following characteristic temporal and spectral features are qualitatively recognizable.

Early Time Range. Located spectrally in the blue end (from 480 to 525 nm) lies the instantaneous negative carotenoid bleach (B_{car}) signal, which is partially overlapped by the negative signal originating from the stimulated emission (SE) from the carotenoid S_2 state between 500 and 620 nm (Figure 4, blue line). The first EADS lives only some tens of femtoseconds before the strong positive carotenoid $S_1 \rightarrow S_n$ ESA dominates. This broad band at 530−700 nm is superimposed with the negative purpurin bleach (Bl_{pur}), with its characteristic features originating from the Q_x and Q_y bands peaking at 583 and 699 nm, respectively (Figure 4, green line). Note that also the features of the purpurin bleach (B_{Pur}) appear during the first few tens of femtoseconds, revealing that at least part of the ET process must occur rapidly right after the excitation.

Medium Time Range. The S_1-S_n ESA_{car} band first narrows and then decays in picosecond timescales. This is accompanied by the partial decline of B_{car} (Figure 4, red and cyan lines). Note here that even after the positive signal due to the ESA_{Car} around 550 nm has disappeared, there clearly is some additional transient state giving rise to the positive signal that lies between

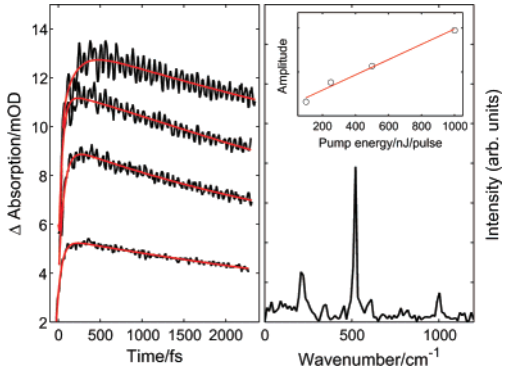

Figure 7. Coherent wave packet oscillations. Left panel: pump−probe traces with increasing pump energies (100, 250, 500, and 1000 nJ/pulse) at 546 nm. Right panel: FFT of the oscillatory pattern at the highest pump energy showing peaks at 217, 530, 795, and 1012 cm^{-1}. Right panel inset: linear pump-energy dependence of the 530 cm^{-1} peak amplitude.

500 and 680 nm (Figure 4, magenta line). The features of the B_{Pur} remain clear.

Late Time Range. Here, a positive signal between 520 and 570 nm, belonging to the carotenoid triplet T_1-T_n ESA_T, rises in nanosecond timescales. At the same time, corresponding growth of Bl_{car} at the blue end of the spectrum and recovery of Bl_{pur} at the red end can be seen.

Oscillations. At the pump intensity used in the pump−probe scans (100 nJ), we also detect subtle signatures of coherent wavepacket oscillations. The oscillations have their maximum amplitude on the red side of the carotenoid ground-state absorption at 520−560 nm and disappear within a few picoseconds. To further study these oscillations, scans with increasing pump intensities up to 1000 nJ/pulse were made. The oscillations were analyzed by fitting a simple exponential function to the early time data at 546 nm (Figure 7, left panel, red curve). The resulting curve was then subtracted from the data, and FFT was then applied to the residual signal, revealing a Fourier spectrum comprised of four frequencies contributing to the oscillatory pattern, 217, 530, 795, and 1012 cm^{-1}, with periods of 150, 63, 42, and 33 fs, respectively. The most pronounced peak is at frequency 530 cm^{-1}, whereas the other peaks were discernible only at higher pulse energies. The amplitude of the oscillations increases linearly with the increasing pump energies, as shown in Figure 7 (see inset of the right panel).

Discussion

The sequential model served as a first step in the data analysis, giving information on the rate constants and general spectral features of the data. In other words, by resolving and comparing the energy-level diagram of the dyad to the one of LH2, it is possible to understand how well the dyad mimics the salient features of the kinetics in LH2. In addition to the branching ratio between the functional channel (ET) and the loss channel (IC), several questions remain. Are there additional dark states involved in the kinetics? Do we see evidence of impulsive Raman scattering (IRS), possibly populating the hot ground state ($HotS_0$)? Is it feasible to resolve a clean enough molecular feedback for the learning-loop experiment as used in LH2 coherent-control experiments? What wavelengths and time positions, if any, are suitable to detect signatures of the IC and ET processes?

Target Analysis. With the previous discussion in mind, the results of a target analysis are discussed here. In this second

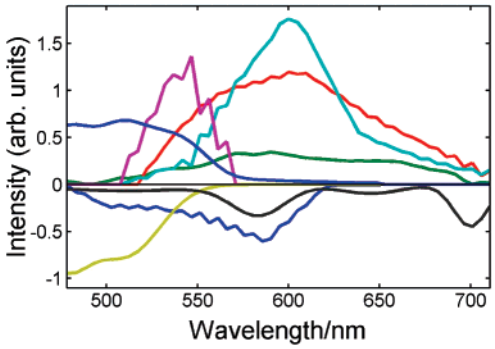

Figure 8. Species associated spectra (SAS) obtained by the target analysis employing the energy-flow diagram of in Figure 9. The following spectral species are presented for the carotenoid moiety: bleach (Bl_{Car}), $S_2 \rightarrow S_0$ stimulated emission (S_2), $HotS_1 \rightarrow S_n$ excited-state absorption ($HotS_1$), $HotS_0 \rightarrow S_2$ excited-state absorption ($HotS_0$), $S_1 \rightarrow S_n$ excited-state absorption (S_1), and $T_1 \rightarrow T_n$ excited-state absorption (T_{Car}). For the purpurin moiety: bleach (Bl_{Pur}), $S_1 \rightarrow S_n$ excited-state absorption ($PurQ_y$).

TABLE 1: Rate Constants of Energy-Flow Pathways

k_{IC} (fs^{-1})	k_{ET} (fs^{-1})	k_1 (fs^{-1})	k_2 (ps^{-1})	k_3 (ps^{-1})	$k_{ISC} + k_4$ (ns^{-1})
$1/110 \pm 5$	$1/50 \pm 4$	$1/290 \pm 15$	$1/7.8 \pm 0.1$	$1/8.3 \pm 0.1$	$1/1.5 \pm 0.2$

step of the data analysis, assumptions based on physical intuition and previous knowledge are put to use, some of which were already presented in the Results, when assigning molecular states to certain spectral features that are depicted by the experimental data and in the EADS. The goal of the target analysis is to find the energy-level diagram, SAS, connections, and rate constants that best describe the measured data. In doing that, one may refer to results previously reported for similar molecules and thus assign certain constraints that are based on information already available.

In principle, target analysis is model testing. Also here, various models, including models with different numbers of states and connections between them, have been tested on the dyad pump−probe data. In the following discussion, the results of the analysis are further elaborated, together with a more detailed discussion over previously presented models for the carotenoids and LH2 complex.

The best model is comprised of seven energy levels (i.e., spectral species): the ground states of carotenoid and purpurin (Figure 8, brown and black lines, respectively); five carotenoid and one purpurin excited states, carotenoid S_2, $HotS_0$, $HotS_1$, S_1, and the triplet (Figure 8, blue, purple, red, cyan, and blue lines, respectively); and purpurin S_1 (Figure 8, green line). The resolved time constants are presented in Table 1. For clarity, the discussion proceeds with the help of the three time regimes already introduced in the previous section.

Early Time Range. The carotenoid S_2 and the carotenoid $HotS_0$ are populated by the laser pulse. Thus, the model includes two states that are initially populated by the pump pulse (S_2 and $HotS_0$). The initially excited population from the S_2 state decays to the vibrationally $HotS_1$ state by internal conversion with a rate constant of $1/110$ fs^{-1}, from which it further undergoes a cooling process that results in the S_1 population with a rate constant of $1/290$ fs^{-1}.

A competing pathway branches from the initially excited S_2 state toward the purpurin excited states. This carotenoid−purpurin singlet−singlet ET has a rate constant of $1/50$ fs^{-1} and gives an ET/IC branching ratio of 69:31 between ET and IC, which is in good agreement with the ratio determined by the steady-state excitation measurements (ET/IC is 67:33).

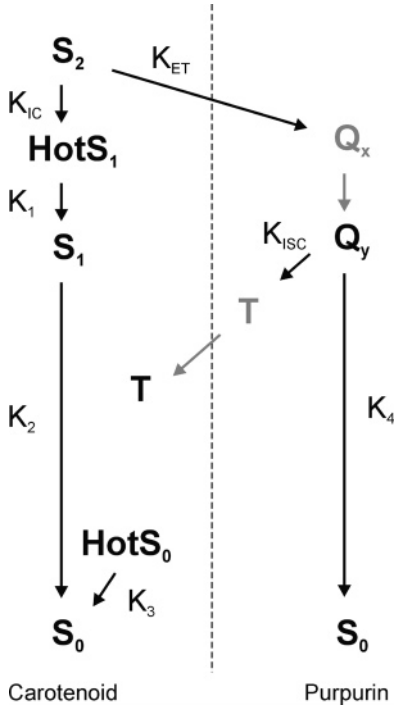

Figure 9. Energy-flow diagram of the bioinspired dyad system.

The carotenoid S_2 excited state has a stimulated emission spectrum located roughly where the carotenoid fluorescence is previously reported to exist.[1] The exact features of the resolved ultrafast spectral band are slightly blurred due to the limited time resolution and a small coherent artifact present in the data.

The vibrational-cooling process of the S_1 state is described by including an additional $HotS_1$ level into the model. Accordingly, the algorithm finds SAS for this intermediate state that extends more broadly than the cooled S_1 SAS, in consequence describing spectral narrowing. The spectral narrowing of the S_1 ESA and the corresponding rate constant is congruent with the work by Polli et al.[9] In their study on rhodopin glucoside in benzyl alcohol and in LH2, they found that S_2 decays to hot S_1 that cools sequentially with two time constants: 50 and 500 fs. Polli et al. used ~10 fs pulses, and likely, the rate constant determined here manifests the lower time resolution used in this study.

It is generally known that the S_1 ESA band of carotenoids contains a pronounced shoulder on the blue side of the peak.[1] This spectral feature has recently come into focus by several groups, and various models (including additional dark states[13−15] or, alternatively, a hot ground state[21,22]) have been presented for carotenoids in solution as well as for the LH2 complex.[18,23] The previous study of the dyad by Macpherson et al. preceded this development and hence did not address these aspects of carotenoid photophysics. Here, the model of Figure 9 includes a carotenoid hot ground state ($HotS_0$), which is populated instantaneously within the excitation pulse by an impulsive stimulated Raman scattering (ISR) process.[24] The population of $HotS_0$ by ISR has been previously reported by Wohlleben et al.[8,25] and by Andersson and Gillbro.[21] Attempts to fit the data with models including an additional dark excited state, lying energetically below the S_2 state and being populated from the S_2 state, were also made. However, the algorithm was unable to find any fit with a comparable χ^2 value as was reached by the model of Figure 9. In light of these results as well as the previous results from using various ultrafast techniques[26] that claim that the general dynamics of the carotenoids are best explained by a model with a $HotS_0$ state, we conclude that the

TABLE 2: Structural, Spectral, and Dynamical Comparison between LH2 and Bioinspired Dyad

	LH2		dyad
	Structure		
donor	carotenoid rhodopin glucoside ($n = 11$)		carotenoid β-carotene derivative ($n = 10$ + benzene ring)
acceptor	bacteriochlorophyll		purpurin
linkage	none		amide bridge
neighbors	9 repeating units in ring structure		none
surrounding	protein		solvent (toluene)
inter-chromophore distance (edge-to-edge) (Å)	3.4 Car-B800 3.6 Car-B850		3.7
	Spectra (absorption)		
donor (nm)	450−540		450-540
acceptor (nm)	Bchl-B800 Bchl-B850	Q_y: 800; Q_x: 592 Q_y: 850; Q_x: 592	Q_y: 699; Q_x: 583; Soret: 439
	Dynamics		
k $S_2 \rightarrow$ *acceptor;* (Φ_{ET}) (fs^{-1})	$S_2 \rightarrow$ Bchl-B800 $S_2 \rightarrow$ Bchl-B850	1/280; (0.2) 1/185; (0.3)	1/50; (0.7)
k_{IC} ($S_2 \rightarrow S_1$); (Φ_{IC}) (fs^{-1})	1/120; (0.49)		1/110; (0.3)
k_{IC} ($S_1 \rightarrow S_0$) (ps^{-1})	1/4.2		1/7.8

carotenoid in the bioinspired dyad system behaves more as a carotenoid in the solvent; no additional excited states were found nor any ultrafast triplet formation via these states is detected as is the case in the LH2 complex.[18]

Medium Time Range. The vibrational cooling from the $HotS_1$ to the S_1 state is followed by the decay of the carotenoid S_1 state to S_0 state by internal conversion with a rate constant of 1/7.8 ps^{-1}. The hot ground state of the carotenoid decays slightly slower (1/8.7 ps^{-1}). In this time regime, the purpurin Q_y ESA, present already at early times, remains effectively unchanged.

The S_1 spectrum has its maximum at 600 nm, and the shape with its long wing extending toward the red is familiar from previous studies on the carotenoid excited state. In natural light-harvesting complexes, both the S_2 and the S_1 states act as donors in the ET. In the case of the LH2 complex, it has been shown that the major part of the energy is transferred directly from the initially excited carotenoid S_2 state and that only a minor part (∼0.5%) of the energy is transferred from the carotenoid S_1 state to the B800 molecules.[3] The stepwise $CarS_1 \rightarrow$ B800 $\rightarrow$ B850 is seen as a rising bleach signal at 860 nm in the pump−probe data. Previously, it has been reported that in the dyad, all of the ET occurs directly from the carotenoid S_2 state.[11] The rise of the negative bleach signal in LH2 at 860 nm may originate from the ET from the carotenoid S_1 state, increasing the amount of excited Bchl molecules, or from the intramolecular internal-conversion process occurring from the carotenoid S_1 state to the carotenoid ground state. The latter case is naturally possible only if the wing of the positive carotenoid $S_1 \rightarrow S_n$ excited-state absorption band extends to overlap with the Bchl bleach, which is not likely the case in LH2. However, in the dyad, the bleach of the purpurin is located some 150 nm closer to the peak of the S_1 ESA, at 700 nm. Hence, it is impossible to say, as to whether the rising bleach in the dyad originates from ET from the carotenoid S_1 state or if it is merely a signature of the decaying wing of the $S_1 \rightarrow S_n$ ESA. Therefore, even using sophisticated global analysis techniques, we cannot rule out the possibility of ET from the carotenoid S_1 state. However, the contribution of this channel would be small: at most only a few percent.

Late Time Range. After the population in the carotenoid S_1 and $HotS_0$ states has decayed, the excess energy left in the system is located in the purpurin Q_y state. The ESA spectrum of the purpurin Q_y state spreads across the spectrum from 500 to 700 nm. From this state, part of the population is relaxed via internal conversion to the ground state, and part of the population undergoes an inter-system crossing (ISC) process from purpurin Q_y to the purpurin triplet state and further a triplet−triplet ET from purpurin to carotenoid $T_{Pur} \rightarrow T_{Car}$ ET. The carotenoid triplet ESA band arises with a rate constant of 1/1.5 ns^{-1}. The ET from the purpurin triplet state to the carotenoid triplet state is fast as compared to the ISC; thus, no population is accumulated in the purpurin T_1 state. Consequently, no spectral signature of the purpurin T_1 state can be resolved from the data.

Comparison: LH2 versus Dyad. The early time dynamics plays the most important role when considering the dyad as a model system to mimic the dynamics of the LH2 complex. The crucial branching occurs from the initially excited S_2 state in less than 100 fs. In LH2, the ratio is known to be 50:50, where the dyad shows a 70:30 branching ratio. The rate constants are comparable; in both systems, the internal conversion occurs in little over 100 fs. Better efficiency of the ET in the dyad is due to faster ET, even though there is only one chromophore accepting the energy (Table 2): LH2: ET ∼110 fs (to B800 1/280 fs^{-1} and to B850 1/185 fs^{-1}) and IC 1/120 fs^{-1} and dyad: ET 1/50 fs^{-1} and IC 1/110 fs^{-1}.

According to the Förster mechanism, the efficiency of the ET depends on the inter-chromophore distance, the relative orientation of the two chromophores, and the overlap between the absorption and the emission spectra. The absorption of the carotenoids is at the same wavelength in both systems, as are the Q_x bands of the accepting molecules (purpurin and Bchls). Accordingly, the rapidly decaying S_2 emission spectra are also likely to exist at the same wavelength in both systems. Hence, the spectral overlap between the donor emission and the acceptor absorption are of the same order in both systems. The edge-to-edge inter-chromophore distances in LH2 are slightly shorter, and the orientation of the dipoles are fixed in the protein matrix. The fact that the dyad depicts faster ET suggests a more favorable average orientation between the chromophores. The involvement of other mechanisms, possibly mediated by the bridge atoms, has also been discussed.[11]

The proposed mechanism behind the enhancement of IC in LH2 by shaped laser pulses involves the excitation of a specific low-frequency mode by an ISR process.[8] A multi-pulse laser field is synchronized to a critical vibrational frequency, or an integer multiple of it, whose activation leads to more rapid internal conversion, thus increasing the efficiency of the loss channel. Interestingly, the dyad depicts coherent wave packet oscillations in the spectral region where the $HotS_0$ is located.

Such oscillations have previously been observed in carotenoids and assigned to ground-state wavepacket motion due to the ISR process within the pump pulse.[9,27] This is one feasible explanation here as well, and the ~530 cm^{-1} peak could be assigned to the beating between the C−C and the C═C stretching modes at 1004 and 1539 cm^{-1}.

Another interpretation could be the involvement of the solvent (toluene) vibrational modes that are somehow coupled to the solute carotenoid. The resolved wavenumbers of the detected three bands agree well with the known toluene FT-IR Raman spectrum, although differing in their relative amplitudes. A similar observation of solvent modes was made by Shimada et al. in a hyper-Raman (HR) scattering experiment on β-carotene solvated in cyclohexane.[28] As is the case in the present study, a mode attributed to the solvent was only detected in the presence of the solute β-carotene but was missing in the neat solvent. The authors ascribed this effect to a solvent induced molecular near field, giving rise to an extra HR band. According to their interpretation, the mixing of the carotenoid S_2 and S_1 states is influenced by the solvent vibrations intervening with the HR process. However, HR scattering is a two-photon process, and the mechanism cannot be the same since the intensity study (see Figure 7) clearly reveals that the amplitude of these oscillations depends linearly on the pump intensity, as expected for an ISR process.[29] Possibly, the mechanism here can be thought to be analogous to surface-enhanced Raman scattering, in that it requires the presence of carotenoid modes and their near-field coupling to the solvent. However, studies varying the concentration and including experiments with deuterated solvents are needed to confirm such a mechanism. We also note that a further influence of the contributing electronic resonance is crucial since a similar solvent band in cyclohexane as detected in a degenerate four wave mixing (DFWM) experiment[30] was only to be detected under resonant excitation conditions and was missing when the solute β-carotene was excited nonresonantly.

Conclusion

We present a detailed time-resolved spectroscopic study on the bioinspired dyad molecule, comparing its structure, spectrum, and dynamics to the LH2 complex from *R. acidophila*. Regardless of the structural simplicity, the dyad mimics the major spectral and kinetic features of the LH2 complex well (see Table 2). The major difference found in the photophysics is the energy flow in the carotenoid moiety, which is consistent with the photophysics of carotenoids in solution rather than in the protein environment of the LH2 complex. In addition, the newly found involvement of the ISR process in the photophysics of the dyad provides further interest in using the dyad in mimicking the coherent-control results obtained in LH2, where ISR is the proposed contributing mechanism.

The caroteno−purpurin dyad is an ideal case for a coherent-control study, having a clear branching of the energy flow between two competing pathways leading to two different processes: IC and ET. With the aid of a global fitting procedure, the underlying spectral and dynamical contributions of the processes were resolved from the data in detail. On the basis of the analysis, clear signals for ET and IC can be resolved in a pump−probe experiment. The amount of energy flowing to the ET channel can be probed around 700 nm and to the IC channel around 610 nm. The sufficient time window for these signals extends from short times to several picoseconds. This provides a reliable and well-characterized feedback signal for future coherent-control experiments, which aim to manipulate the efficiency of these processes.

Acknowledgment. Liam McDonnell and Peter van der Walle are thanked for useful discussions. This work is part of the research program of the Stichting voor Fundamenteel Onderzoek der Materie, which is financially supported by the Nederlandse Organisatie voor Wetenschappelijk Onderzoek.

References and Notes

(1) Polivka, T.; Sundstrom, V. *Chem. Rev.* **2004**, *104*, 2021.

(2) Sundstrom, V.; Pullerits, T.; van Grondelle, R. *J. Phys. Chem. B* **1999**, *103*, 2327.

(3) Macpherson, A. N.; Arellano, J. B.; Fraser, N. J.; Cogdell, R. J.; Gillbro, T. *Biophys. J.* **2001**, *80*, 923.

(4) Polivka, T.; Zigmantas, D.; Herek, J. L.; He, Z.; Pascher, T.; Pullerits, T.; Cogdell, R. J.; Frank, H. A.; Sundstrom, V. *J. Phys. Chem. B* **2002**, *106*, 11016.

(5) Herek, J. L.; Wohlleben, W.; Cogdell, R. J.; Zeidler, D.; Motzkus, M. *Nature (London, U.K.)* **2002**, *417*, 533.

(6) Gust, D.; Moore, T. A.; Moore, A. L.; Liddell, P. A. Synthesis of carotenoporphyrin models for photosynthetic energy and electron transfer. In *Carotenoids Part A: Chemistry, Separation, Quantitation, and Antioxidation*, 213th ed.; Packer, L., Ed.; Academic Press: San Diego, 1992; p 87.

(7) McDermott, G.; Prince, S. M.; Freer, A. A.; Hawthornthwaite-Lawless, A. M.; Papiz, M. Z.; Cogdell, R. J.; Isaacs, N. W. *Nature* **1995**, *374*, 517.

(8) Wohlleben, W.; Buckup, T.; Herek, J. L.; Motzkus, M. *ChemPhysChem* **2005**, *6*, 850.

(9) Polli, D.; Cerullo, G.; Lanzani, G.; De Silvestri, S.; Hashimoto, H.; Cogdell, R. J. *Biophys. J.* **2006**, *90*, 2486.

(10) Fuss, W.; Haas, Y.; Zilberg, S. *Chem. Phys.* **2000**, *259*, 273.

(11) Macpherson, A. N.; Liddell, P. A.; Kuciauskas, D.; Tatman, D.; Gillbro, T.; Gust, D.; Moore, T. A.; Moore, A. L. *J. Phys. Chem. B* **2002**, *106*, 9424.

(12) Berera, R.; Herrero, C.; van Stokkum, I. H. M.; Vengris, M.; Kodis, G.; Palacios, R. E.; van Amerongen, H.; van Grondelle, R.; Gust, D.; Moore, T. A.; Moore, A. L.; Kennis, J. T. M. *Proc. Natl. Acad. Sci. U.S.A.* **2006**, *103*, 5343.

(13) Papagiannakis, E.; Kennis, J. T. M.; van Stokkum, I. H. M.; Cogdell, R. J.; van Grondelle, R. *Proc. Natl. Acad. Sci. U.S.A.* **2002**, *99*, 6017.

(14) Larsen, D. S.; Papagiannakis, E.; van Stokkum, I. H. M.; Vengris, M.; Kennis, J. T. M.; van Grondelle, R. *Chem. Phys. Lett.* **2003**, *381*, 733.

(15) Gradinaru, C. C.; Kennis, J. T. M.; Papagiannakis, E.; van Stokkum, I. H. M.; Cogdell, R. J.; Fleming, G. R.; Niederman, R. A.; van Grondelle, R. *Proc. Natl. Acad. Sci. U.S.A.* **2001**, *98*, 2364.

(16) Holzwarth, A. R. Data analysis of time-resolved measurements. In *Biophysical Techniques in Photosynthesis*, 1st ed.; Amesz, J., Hoff, A. J., Eds.; Kluwer Academic Publishers: Dordrecht, The Netherlands, 1996; Vol. 3, p 75.

(17) van Stokkum, I. H. M.; Larsen, D. S.; van Grondelle, R. *Biochim. Biophys. Acta* **2004**, *1657*, 82.

(18) Wohlleben, W.; Buckup, T.; Herek, J. L.; Cogdell, R. J.; Motzkus, M. *Biophys. J.* **2003**, *85*, 442.

(19) Hansen, N.; Ostermeier, A. *Evol. Comput.* **2001**, *9*, 159.

(20) Fanciulli, R.; Willmes, L.; Savolainen, J.; van der Walle, P.; Bäck, T.; Herek, J. L. *Evolution Strategies for Laser Pulse Compression*, Artificial Evolution, 8th International Conference, Evolution Artificielle, EA 2007, Lille, France, October 29−31, 2007; Revised Selected Papers, Lecture Notes in Computer Science; Springer: Berlin/Heidelberg.

(21) Andersson, P. O.; Gillbro, T. *J. Chem. Phys.* **1995**, *103*, 2509.

(22) Buckup, T.; Savolainen, J.; Wohlleben, W.; Herek, J. L.; Hashimoto, H.; Correia, R. R. B.; Motzkus, M. *J. Chem. Phys.* **2006**, *125*, 194505.

(23) Papagiannakis, E.; van Stokkum, I. H. M.; Vengris, M.; Cogdell, R. J.; van Grondelle, R.; Larsen, D. S. *J. Phys. Chem. B* **2006**, *110*, 5727.

(24) Yan, Y.-X.; Gamble, J.; Edward, B.; Nelson, K. A. *J. Chem. Phys.* **1985**, *83*, 5391.

(25) Wohlleben, W.; Buckup, T.; Hashimoto, H.; Cogdell, R. J.; Herek, J. L.; Motzkus, M. *J. Phys. Chem. B* **2004**, *108*, 3320.

(26) Buckup, T.; Wohlleben, W.; Savolainen, J.; Heinz, B.; Hashimoto, H.; Cogdell, R. J.; Herek, J. L.; Mozkus, M. Energy flow in carotenoids, studied with pump−deplete−probe, multiphoton, and coherent control spectroscopy. In *Ultrafast Phenomena XIV*; Springer: Berlin, 2005; p 368.

(27) Cerullo, G.; Lanzani, G.; Zavelani-Rossi, M.; De Silvestri, S. *Phys. Rev. B: Condens. Matter Mater. Phys.* **2001**, *63*, 241104.

(28) Shimada, R.; Hideaki, K.; Hamaguchi, H.-o. *J. Raman Spectrosc.* **2006**, *37*, 469.

(29) Dhar, L.; Rogers, J. A.; Nelson, K. A. *Chem. Rev.* **1994**, *94*, 157.

(30) Hauer, J.; Skenderovic, H.; Kompa, K. L.; Motzkus, M. *Chem. Phys. Lett.* **2006**, *421*, 523.